Proceedings of the XII International Symposium on Dynamic Problems of Mechanics (DINAME 2007),
Varoto, P. S. and Trindade, M. A. (Editors), ABCM, Ilhabela, SP, Brazil, February 26 - March 2, 2007

IDENTIFYING OIL INSTABILITY PHENOMENA IN ROTORS USING NONLINEAR TECHNIQUES ANALYSIS

Michalski, M. A. C. [1], Moreno, Y. M. B. [2], Rocha, R. O. [1], Zindeluk, M. [2]

[1] Cepel – Centro de Pesquisa em Energia Elétrica – Av. Jequitibá s/n – Cidade Universitária, Ilha do Fundão – Rio de Janeiro, RJ – Brasil – CEP: 21944-970

[2] LAVI – COPPE/UFRJ –Sala I-130 – Centro de Tecnologia – Av. Jequitibá s/n – Cidade Universitária, Ilha do Fundão – Rio de Janeiro, RJ – Brasil – CEP: 21945-970

Abstract: The present work studies the application of simple nonlinear techniques – the Poincaré Map and the Bifurcation Diagram Analysis – experimentally obtained in the identification of oil instability phenomena – as oil whirl and oil whip – that very often occur in machines supported by hydrodynamic journal bearings. Considering two test rigs – one horizontal and another vertical – with flexible rotors derived from the Jeffcott model supported by plain journal bearings, the disk displacement at two orthogonal directions is observed, so the orbit and Poincaré section can be obtained in each case. After the data acquisition under several spin velocities, the Bifurcation diagram is also obtained. From the dispersion of the points and bifurcations found in the maps, conditions of stability, transition and instability, directly associated to the occurrence of the oil phenomena can be characterized. The results from both rigs are also compared.

Keywords: rotordynamics, machine monitoring, nonlinear dynamics.

INTRODUCTION

The study presented in this work belongs to a research line where the use of classical signal processing tools in the identification and monitoring of oil instabilities phenomena is complemented with simple nonlinear tools, as the Poincaré Section, the Phase Portraits and also the Bifurcation Diagram.

These alternative methods allow a more complete approach, as long as the nature of fluid instability problems in rotation machines is essentially nonlinear. The quality of the problem analysis can be improved and a new range of solutions can be obtained.

This work follows other ones presented before, where the nonlinearity is considered only in the fluid bearings hydrodynamic. Wang and Wang (2005) presented a nonlinear dynamic and bifurcation analysis of short aerodynamic journal bearings, where a numerical analysis was made comparing the results of the system state trajectory, Poincaré maps, power spectra and bifurcation diagrams. In Michalski, Zindeluk and Rocha (2006), the influence of journal bearing axial grooves on the dynamic behavior of horizontal rotors has been experimentally studied and the Poincaré map analysis was used as an alternative tool to complement the classical orbit and FFT analysis. Recently, in Bachschimid and Pennacchi (2006), was published a work proposing a nonlinear experimental detection of oil whirl in horizontal rotors using a new index, called occupation grade, based in the Poincaré map analysis.

Previously, Adiletta, Guido and Rossi (1997) presented a work divided in two parts where the nonlinear dynamics of a rigid unbalanced rotor in journal bearings analysis was presented in theoretical and experimental aspects. In this case, nonlinearities were considered not only in the bearings but also in the model trigonometric coordinates. The bifurcation diagram analysis was used only in the theoretical part of the work. This tool is very useful when a rotor system is analyzed under several different conditions, but is generally presented as a part of numerical model analysis, like Ping et al. (2004), where the nonlinear dynamic behavior of a rotor-bearing system is based in a continuum model.

Considering the successful use in previous works of nonlinear tools in rotordynamic phenomenon analysis, this paper brings an experimental use of the Poincaré map, Bifurcation diagram, the classical FFT analysis and the occupation grade identifying oil instabilities in two different rotors supported by plain journal bearings. Also, these rotors behaviors can be compared with the same tools.

The Experimental System

In this part of the paper, the test rigs used will be described in a brief way. For more details, the works of Murta (2000), Abrantes and Michalski (2002) and Michalski (2004) are the best references, presenting the test rigs design, building and evaluation.

Both rotors used are based in a Jeffcott model with a single disk clamped in a flexible shaft and positioned in the middle of the gap between two plain journal bearings. The shaft and the disk are made in steel SAE 1045. The shaft total length is 800 mm in the horizontal rig and 600 mm in the vertical one. In both cases the shaft diameter is 8,0 mm.

The disks diameter is 150 mm and the thickness is 15 mm. The bearings were manufactured in bronze with the inside diameter of 8,1 mm and the length of 8,0 mm. The radial clearance is about 0,1 mm.

The oil used in the horizontal test rig is the Lubrax Industrial HR-32-EP (ISO Grade 32), with absolute viscosity equals to 0.0261 N.s/m². The temperature during the acquisition period in the tests was 40 ºC. In the vertical test rig, it was used the Ipiranga Ipitur AW 32 (ISO Grade 32) with absolute viscosity equals to 0.274 N.s/m². The temperature during the tests was 38 ºC.

The horizontal rotor was driven by an electric motor WEG 0,33 HP, two poles, with an AC converter WEG ML-2.6/1AC. 200-240; the vertical one used an electric motor Erbel 0,25 HP, two poles, with an AC converter.

Inductive analogue sensors Balluff BAW 018-PF-1-K measured the disk displacement in the radial direction, with 90º between them. In the vertical rotor, the sensors measured the principal displacement directions. In the horizontal rig, as a matter of building specifications, the sensors were rotated 45º from the principal displacement axis. So, the principal displacement directions were formed by a composition between the two measured axes.

The tachometer in the horizontal rig was an optical emitter/receptor working with an aluminum disk with a single hole positioned in the electric motor shaft. In the vertical one, another inductive sensor positioned in the axial direction and a small metal plate fixed in the disk were used for this task. The experimental data was acquired using a laptop with NI DAQCard 6024E I/O with 200 kS/s, a connector block BNC-2110 and a shielded cable from National Instruments.

The acquisition frequency was 2048 Hz and the total number of points acquired was 20980, discarding the first 500 points, what means 10 seconds in the real acquisition duration. The programs used to acquire and analyze the signals were developed in LabView. The signals were filtered at 300 Hz and the highest frequency presented was 200 Hz. With the acquisition frequency used, there were no aliasing problems, as presented in Ripper (1994), and no need of analogical filters. The entire experimental tests were done under these conditions.

The data was acquired in steady-state conditions in both rigs. In the horizontal rotor the acquisition began with a spin frequency of 5 Hz and stopped at 100 Hz, in steps of 5 Hz. In the vertical one, the lowest spin frequency was also 5 Hz and the maximum value was 70 Hz. In this case the steps were not fixed, but varying from 1 to 5 Hz, depending on the stability condition.

Analysis Methodology

Once the data acquisition is made, the signals are analyzed using the classical FFT and the orbit analysis with the Poincaré section for each rotational speed. For each test rig, two bifurcation diagrams are also presented, one for each displacement direction measured. An occupation grade plot is also presented in each case, showing the rotor behavior evolution with the rotational speed increment.

There is not a general method to obtain a Poincaré map (Savi, 2006). In this work the study of orbits near a periodic behavior was used and unbalance was considered the unique external force in the system. Once the tachometer assures the real spin frequency, this value is used to “resample” the signals and build the Poincaré map. Therefore, instead of a continuous plot, the orbit is converted in a discrete plot.

The bifurcation diagram is used to identify some parameters influence in the system response, presented by a stroboscopic distribution. In this work, the spin frequency is the chosen parameter and, as the signal acquisition was performed under a steady-state condition in very close steps, it is possible to see the global influence of the speed variations in the rotor behavior, what means to identify the oil instability phenomena.

As the Poincaré map and the bifurcation diagram use in this work the same parameter, they become complementary in the given information. When the rotor has a steady-state motion with a period equal to the period of the forcing function, all points in the Poincaré section should be superimposed on each other (Gent, 1999), as in the bifurcation diagram. However, a nonlinear system excited by a harmonic forcing function can, in certain cases, exhibit what is usually called a subharmonic oscillation, as occurs with rotors undergoing into oil whirl or oil whip. When these phenomena are expressive, the fundamental motion frequency can be smaller than that of the forcing function, once the subharmonic frequency amplitude can be greater than the rotational frequency amplitude. In this condition, the Poincaré map and the bifurcation diagram present several points, representing the phenomenon nonlinearity.

Due to imperfections in the experimental system, signal noise, and some unexpected frequencies in the spectrum, the traced orbit is never a single well defined line but a straight zone, even near balance resonance speeds. In this case, the Poincaré map is composed by a single or many point clouds and the bifurcation diagram presents several points forming a single line or several segments. This can bring some difficulties to the phenomena comprehension.

Experimental Results

In this section the experimental results will be presented. First, in Fig. 1, the horizontal rotor orbit and Poincaré map for several spin frequencies. Then, in Fig. 2 (a and b) the FFT graphs related to each orbit presented before are illustrated.

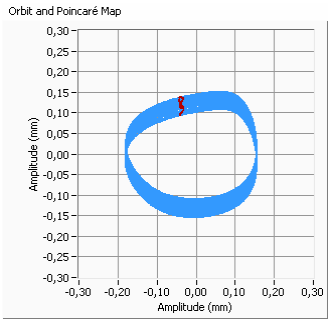

5Hz

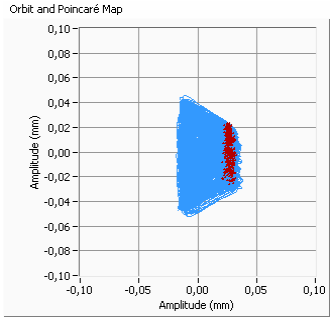

40Hz

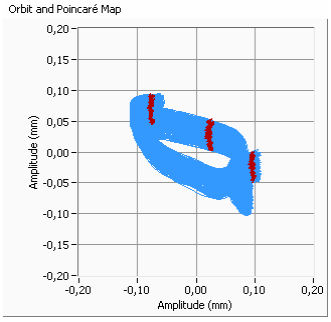

65Hz

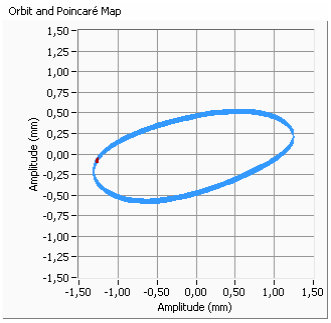

25 Hz

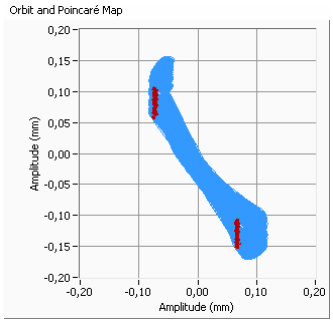

45 Hz

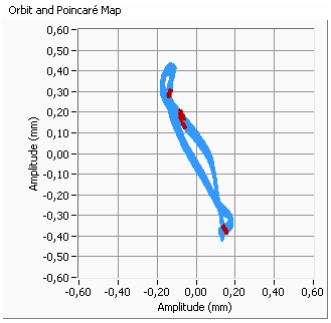

75 Hz

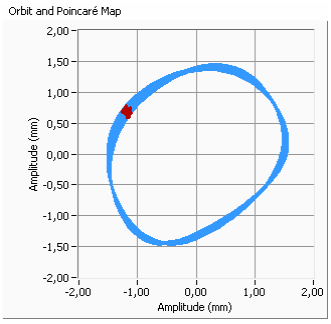

30 Hz

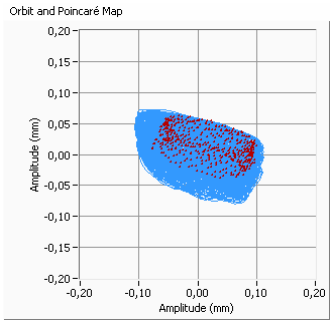

50 Hz

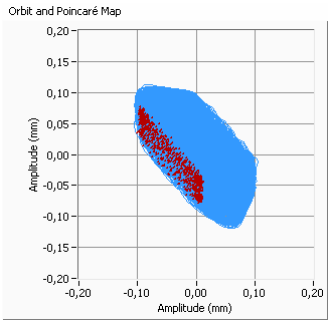

80 Hz

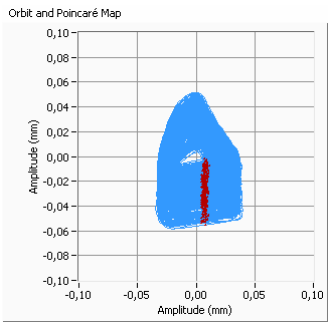

35 Hz

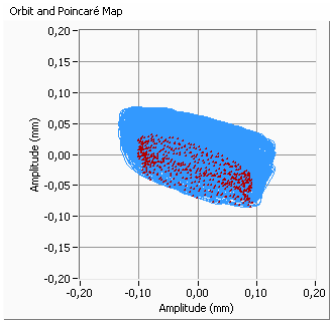

60 Hz

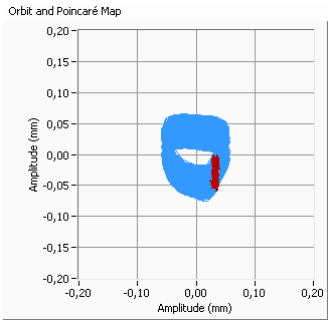

85 Hz

Figure 1 – Horizontal Rotor orbit and Poincaré map in several spin frequencie

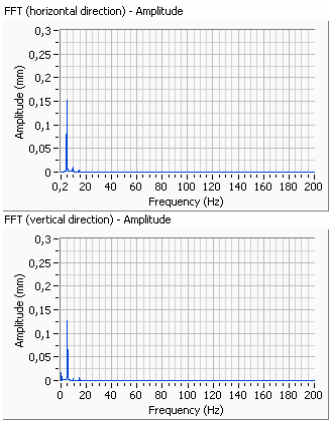

5Hz

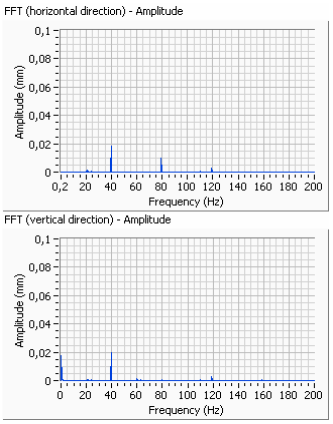

40Hz

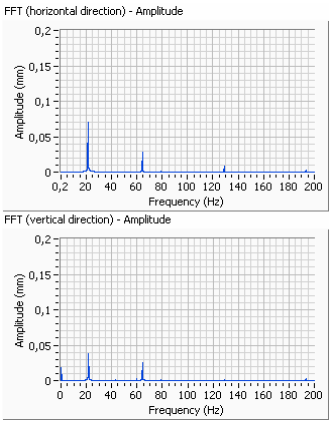

65Hz

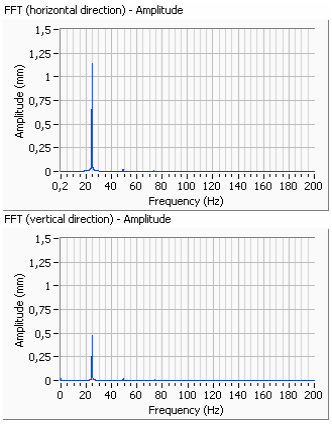

25 Hz

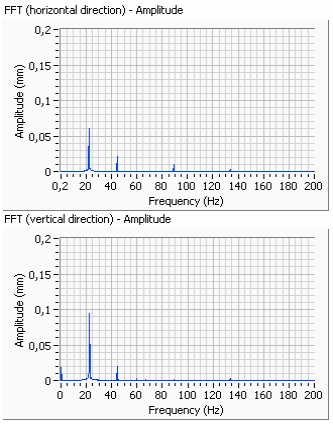

45 Hz

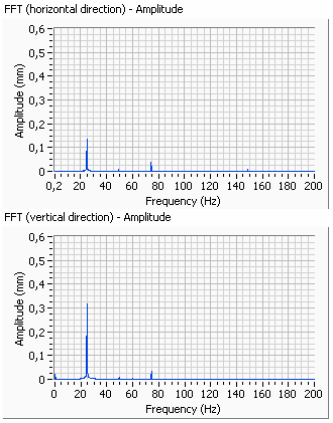

75 Hz

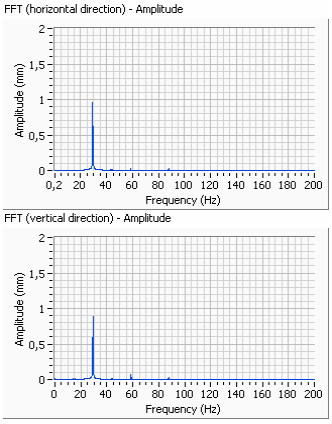

30 Hz

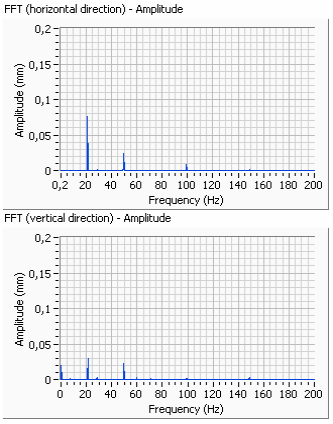

50 Hz

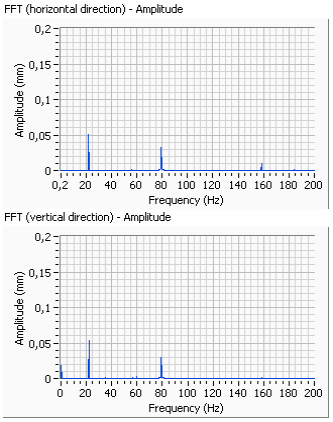

80 Hz

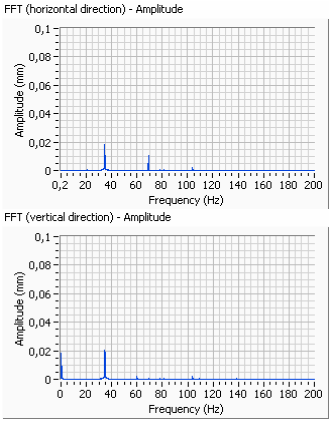

35 Hz

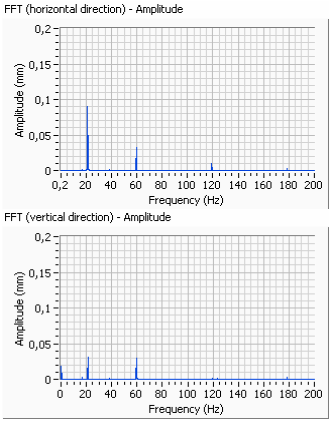

60 Hz

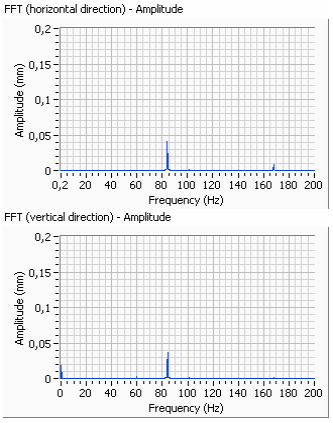

85 Hz

Figure 2 – Horizontal Rotor FFT in several spin frequencies

In this case, the named horizontal and vertical directions are compositions between the x and y measured axis, since they are rotated 45º from the principal displacement axis.

With the graphs analysis, it is possible to say that the rotor first resonance speed is near 30 Hz. Between this spin frequency and 35 Hz, the orbit amplitude reduces significantly, representing the balance resonance speed crossing (Lalanne and Ferraris, 1998).

After the balance resonance speed crossing, the oil whirl phenomenon begins to be noticeable. As described by Muszynska (1986), above the first balance resonance speed, the synchronous forced vibration decays. However, in the FFT plots the amplitude near half the rotational speed value is not significantly yet. The rotor behaviors between a stable condition, where the inertial forces dominate the rotor motion, and an unstable condition, where the fluid forces begin to act. This transitory state will continue until the rotor speed reaches a value near twice the balance resonance speed.

It is interesting to observe the changes from 40 Hz to 80 Hz, when it is evident the oil whirl. The amplitude near the first balance resonance speed is much higher than the amplitude of the rotor rotational speed. In the Poincaré map this behavior change is represented by a bifurcation. Now, in some cases, instead of one single attractor, two or more point clouds are presented (near 45 Hz and from 65Hz to 75Hz). In other cases (from 50Hz to 60 Hz and near 80 Hz) a single large point cloud is present, demonstrating a transient condition.

Fig. 3 and Fig. 4 show the horizontal rotor bifurcation diagrams where all this changes are noticeable, in the two orthogonal directions measured. In the vertical axis it is illustrated the rotor normalized amplitude (adimensional) in the direction considered and in the horizontal axis it is shown the rotational speed, in Hz.

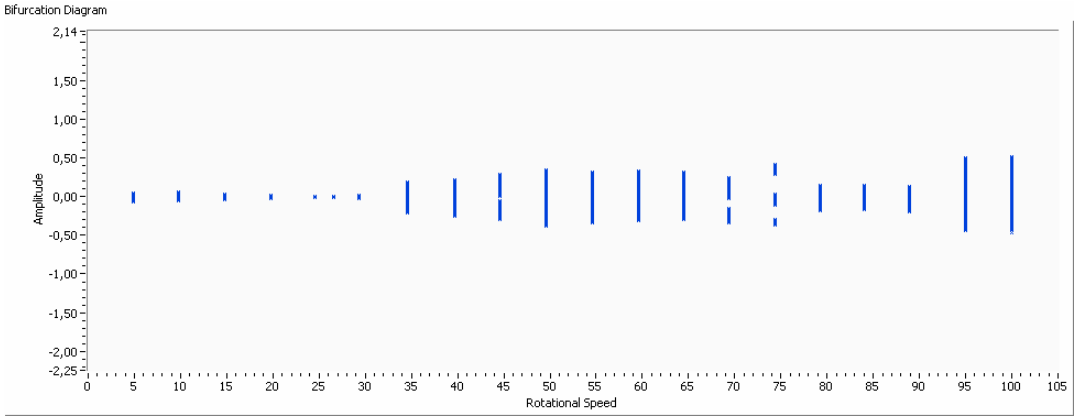

Figure 3 – Horizontal rotor bifurcation diagram – x direction

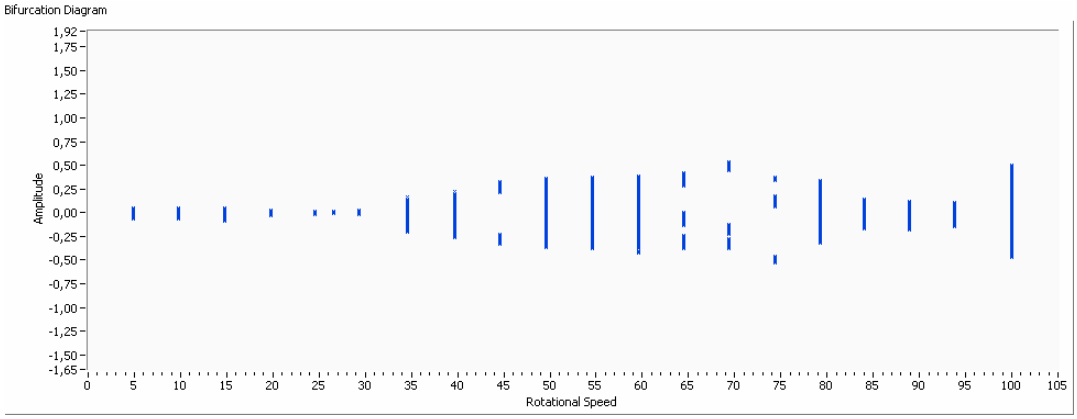

Figure 4 – Horizontal rotor bifurcation diagram – y direction

Fig. 5 shows the occupation grade versus the spin frequency. The instability limits are noticeable, beginning at 40 Hz and ending at 85 Hz, with a peak at 75 Hz, when the oil whirl excites the rotor in its maximum unstable condition.

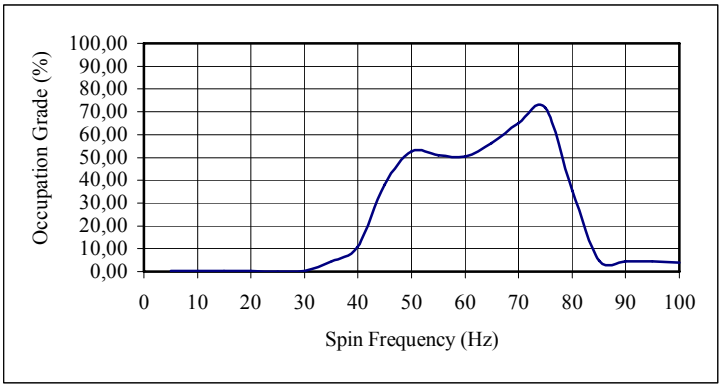

Figure 5 – Horizontal rotor occupation grade versus spin frequency

Next, in Fig. 6, the vertical rotor orbits and Poincaré maps for several spin frequencies.

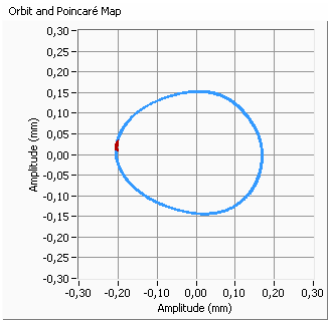

5Hz

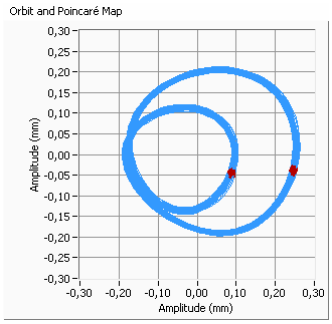

40 Hz

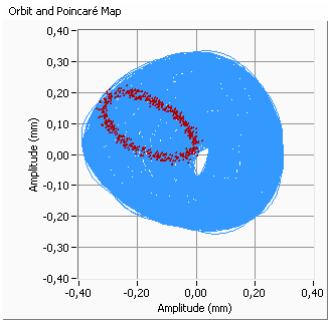

57 Hz

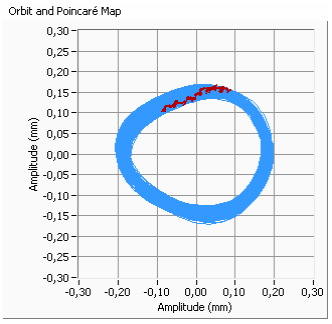

25 Hz

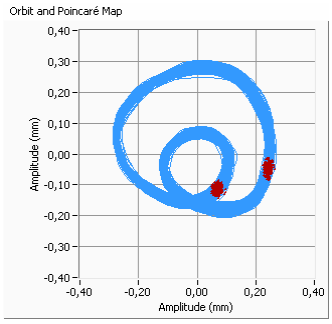

50Hz

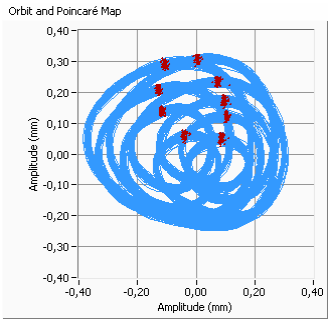

58 Hz

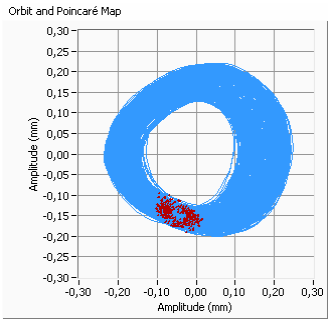

35 Hz

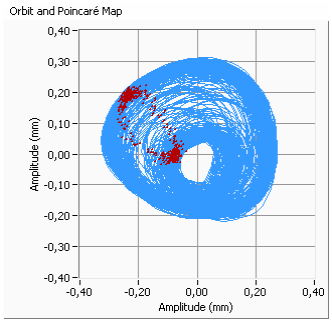

51 Hz

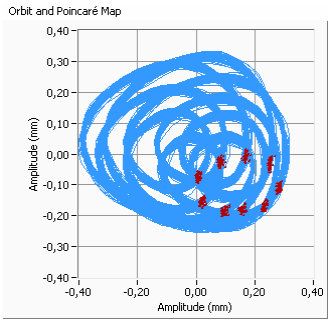

59 Hz

Figure 6a – Vertical Rotor orbits and Poincaré maps in several spin frequencies

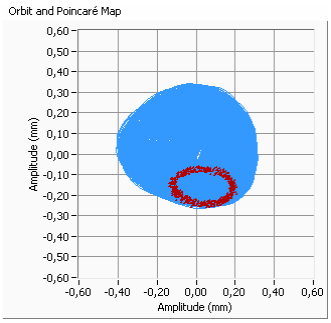

60 Hz

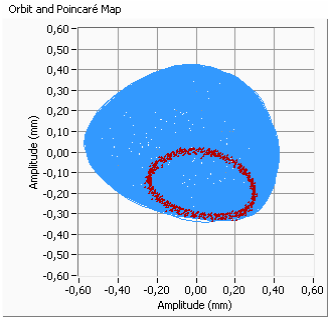

69 Hz

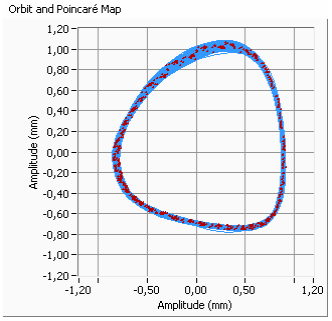

70 Hz

Figure 6b – Vertical Rotor orbits and Poincaré maps in several spin frequencies

As a vertical rotor does not have any force acting to stabilize the rotor, as the self weight does in the horizontal rotor case, the changes in the behavior between a stable and unstable condition are much more sensible. The Poincaré map shows very different configurations with a very little rotational speed change.

Another point observed in this rotor behavior is the fact that the unbalance forces are very weak, and the direct consequence is the unnoticed balance resonance speed crossing. However, when the oil instability is strong and the oil whirl becomes oil whip at 70 Hz, the first resonance speed can be known, and it is probably between 30 Hz and 35Hz (as shown in Genta, 1999, the oil spin frequency is near 45% to 48% of the rotor frequency).

Following, in Fig. 7, the FFT graphs related to each orbit presented before. In this case, the named horizontal and vertical directions are both in the horizontal plain and coincide with the x and y measured directions.

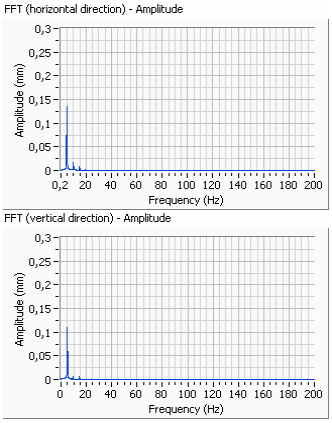

5Hz

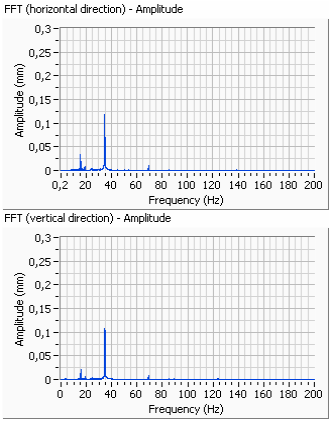

35Hz

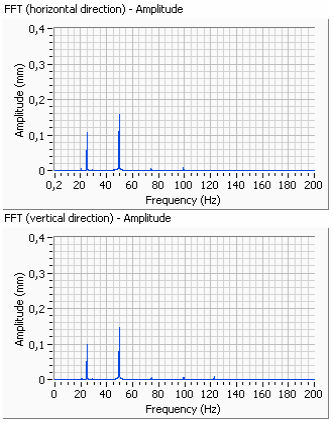

50Hz

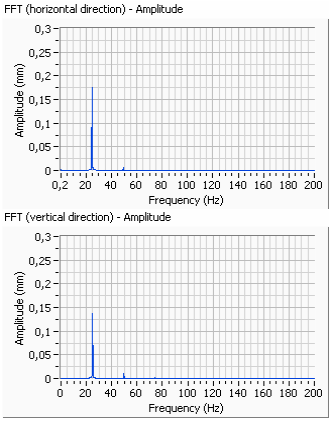

25 Hz

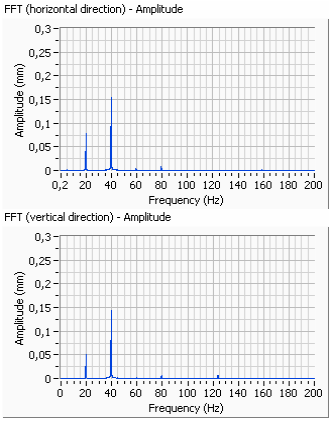

40 Hz

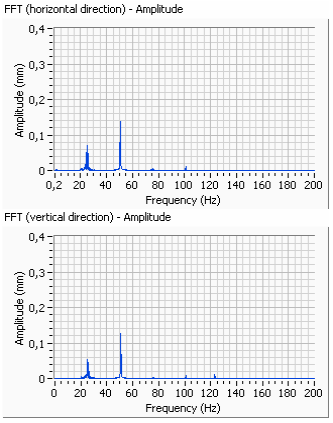

51 Hz

Figure 7a – Vertical Rotor FFT in several spin frequencies

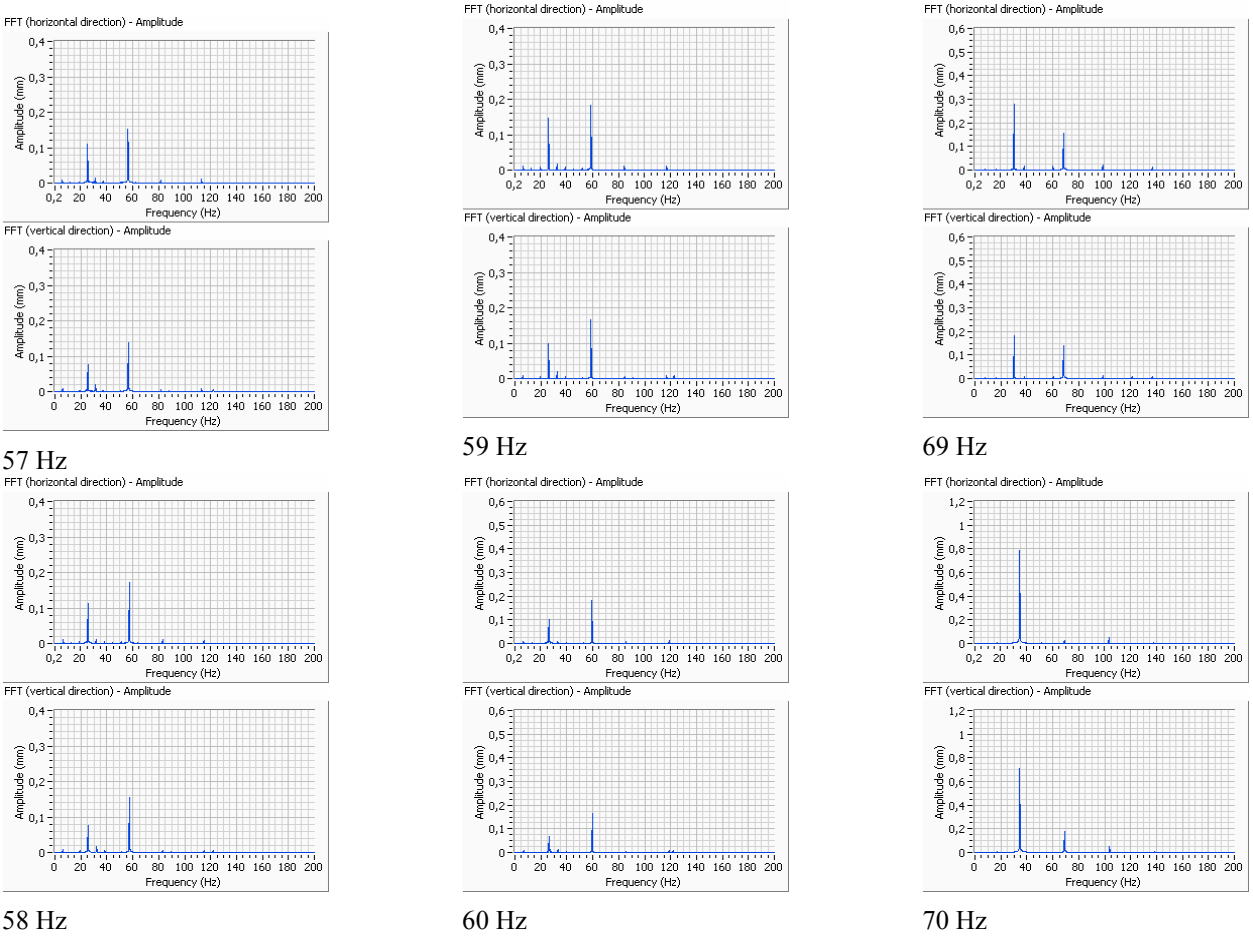

Figure 7b – Vertical Rotor FFT in several spin frequencies

After analyzing the FFT plots at 35 Hz, it is observed that the oil whirl became noticeable, since the amplitude of the frequency near the half part of the rotor spin frequency value increased. The oil spin frequency amplitude was lower than the rotor one until it reached 60 Hz, when the rotor whirl became stronger. Then, at 70 Hz the oil whirl turned into oil whip and the rotor behavior became extremely unstable. During the experimental tests, the displacements amplitudes under this condition were so high that the rotor shaft would begin to bump against the bearing wall unless it had been shut down.

Fig. 8 and Fig. 9 present the vertical rotor bifurcation diagram of the orthogonal directions measured. Fig. 10 exhibits the occupation grade versus the spin frequency plot. In all these cases, it is evident the rotor behavior change, when the oil whip begins to act, especially in the occupation grade plot, when the index suddenly reaches a very high value.

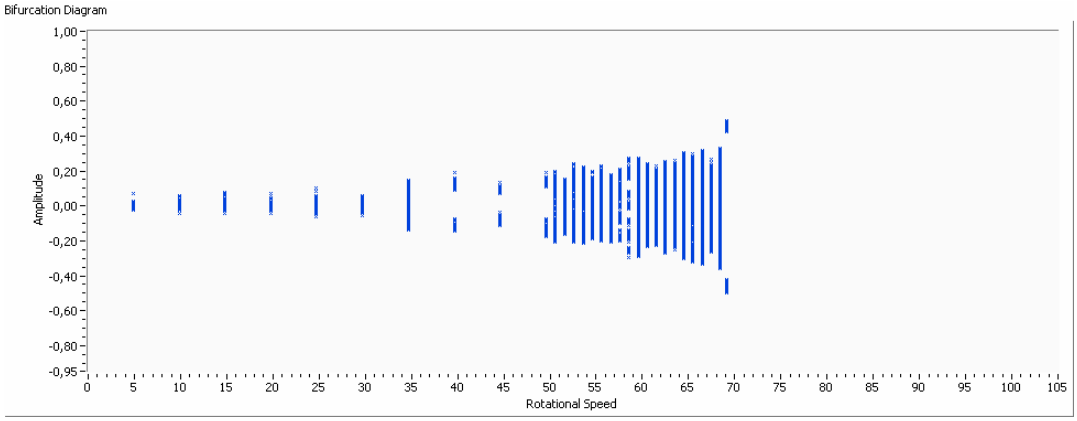

Figure 8 – Vertical rotor bifurcation diagram – x direction

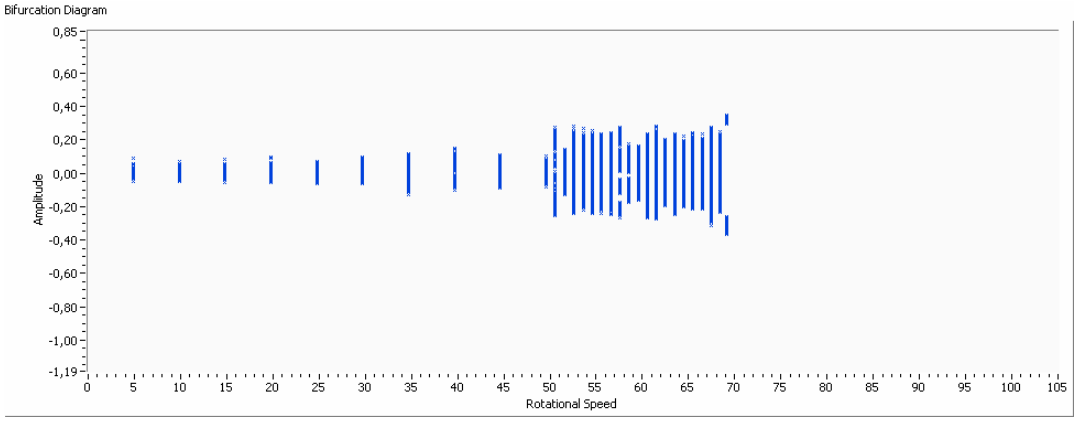

Figure 9 – Vertical rotor bifurcation diagram – y direction

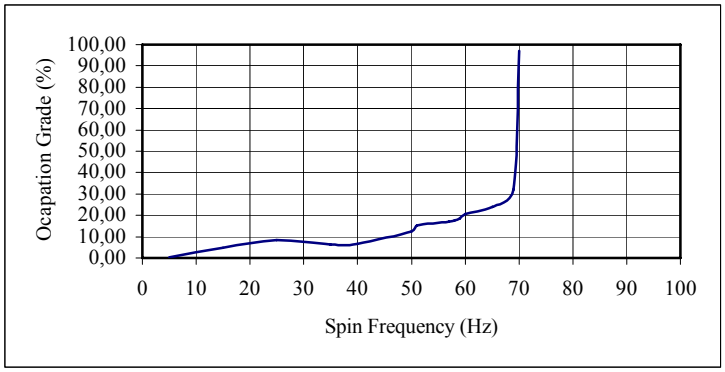

Figure 10 – Vertical rotor occupation grade versus spin frequency

Conclusions

Analysing the two rotors results, it is clear how the nonlinear tools used are efficient in order to evidence the oil instability phenomenon, especially in the vertical test rig case, where no restoration forces are present (as the rotor self-weight) and the system external forces are weak (as the unbalance forces).

Considering only the horizontal rotor, it is very interesting to see how the oil whirl evolutes, changing the rotor behavior. The FFT analysis simply shows the amplitude changes between the rotor spin frequency and its half sub-harmonic. However, the Poincaré map, plotted with the rotor orbit, presents a slow and clear change as the rotor rotational speed increases. The rotor is in a stable state during its first resonance speed crossing and up to 35 Hz, there are no unstable behavior symptoms. But, at 40 Hz the rotor is in a transient condition, which becomes an unstable state, from 45 Hz to 75 Hz, where the bifurcations appear. The same is noticeable in the Bifurcation Diagram. In this period, the bifurcations are intercalated by unstable conditions, as expected. Then, at 80 Hz the rotor begins to enter into a stable state again. The oil whirl was evident but never turned into oil whip. This happens because in the horizontal rotor, its self-weight acts as restoration force, stabilizing the system.

The horizontal rotor occupation grade diagram shows basically two zones: one, with a lower level, where the oil whirl does not happen and another, with higher values, where the oil whirl is present.

On the other hand, considering the vertical rotor, the behavior changes appear very fast with a very small shift in the spin frequency. Until 35 Hz the rotor presents a very stable state, that the first resonance speed crossing is practically unnoticeable. The unbalance forces are extremely small and the system dump is high enough to eliminate any expressive amplitude increase. At 35 Hz, as in the horizontal rotor, the oil whirl begins to be apparent. But, in this case, there is no transient state, and suddenly at 40 Hz the first bifurcation appears. The rotor symmetry is evident even in the orbit plot.

Until 60 Hz, the oil whirl consequences are very weak and the rotor runs in an unstable state without any kind of damage. The displacement amplitude is quite stable and the hydrodynamic forces are even smaller than the unbalance forces. However, until 69 Hz these forces increase and, the oil whirl consequences are stronger. The collapse happens between 69 Hz and 70 Hz. The oil whirl becomes oil whip and the rotor trajectory is no more controllable or predictable. The shaft begins to hit the amplitude limiter and the rotor needs to be turned of.

In the vertical rotor occupation grade plot, this change is represented by a very abrupt rise in the index value. This index does not reach a maximum level in this case.

Although the test rigs are far from being considered equal they are very similar. The rotors have a very close behavior until the hydrodynamic forces act with enough power to make the systems unstable. The major difference between them is the presence of a restoration force only in the horizontal rotor. This single, but not negligible, difference is enough to inhibit the oil whip and keep the machine stable and controllable during a slow acceleration.

ACKNOWLEDGMENTS

The authors would like to thank the support from CEPEL (Electric Energy Research Center) and LAVI (Acoustic and Vibration Laboratory – COPPE/UFRJ) for the support in this work

REFERENCES

Abrantes, M. V. G. D. and Michalski, M. A. C., "Projeto e Construção de uma Bancada Experimental para Estudos em Dinâmica de Rotores Horizontais", College Study Final Dissertation, Engineering College, Mechanical Engineering Department, UFRJ, Rio de Janeiro, RJ, Brasil.

Adiletta, G.; Guido, A. R. and Rossi, C., 1997, "Nonlinear Dynamics of a Rigid Unbalanced Rotor in Journal Bearings, Part I: Theoretical Analysis", Nonlinear Dynamics, Vol. 14, pp. 57 – 87.

Adiletta, G.; Guido, A. R. and Rossi, C., 1997, "Nonlinear Dynamics of a Rigid Unbalanced Rotor in Journal Bearings, Part II: Experimental Analysis", Nonlinear Dynamics, Vol. 14, pp. 157 – 189.

Bachschimid, N. and Pennacchi, P., 2006, "Advances in Vibration Control and Diagnosis", Ed. Polimetrica – International Science Publisher, Monza / Milan, Italy.

Genta, G., 1999, "Vibration of Structures and Machines – Practical Aspects", Third Edition, Springer-Verlag New York Inc.

Lalanne, M.; Ferraris, G., 1998, "Rotordynamics Prediction in Engineering", Second Edition, John Wiley & Sons Ltd.

Michalski, M. A. C., 2004, "Análise Teórico Experimental do Comportamento Dinâmico de um Rotor Horizontal Suportado por Mancais Hidrodinâmicos", M. Sc. Theses, COPPE/UFRJ, Rio de Janeiro, RJ, Brasil.

Michalski, M. A. C.; Zindeluk, M. and Rocha, R. O., 2006, "Influence of journal bearing axial grooves on the dynamic behavior of horizontal rotors", Shock and Vibration, Vol. 13.

Murta, M. S., 2000, "Projeto, Construção e Avaliação Dinâmica de um Rotor Vertical Suportado em Mancais Hidrodinâmicos", M. Sc. Theses, COPPE/UFRJ, Rio de Janeiro, RJ, Brasil.

Muszynska, A., 1986, "Whirl and Whip – Rotor/Bearing Stability Problems", Journal of Sound and Vibration, Vol. 110, No. 3, pag. 443 – 462.

Ping, J. J.; Guang, M.; Yi, S.; Bo, X. S., 2004, "On the non-linear dynamic behavior of a rotor-bearing system", Journal of Sound and Vibration, Vol. 274, pp. 1031 – 1044.

Ripper, G., 1994, "Análise Modal: Teoria e Prática Aplicadas em um Sistema para Controle Ativo de Vibrações", M. Sc. Theses, COPPE/UFRJ, Rio de Janeiro, RJ, Brasil.

Savi, M. A., 2006, "Dinâmica Não-Linear e Caos", E-Papers Serviços Editoriais, Rio de Janeiro, RJ, Brasil.

Wang, J. S. and Wang, C. C., 2005, "Nonlinear dynamic and bifurcation analysis of short aerodynamic journal bearings", Tribology International, Vol. 38, pp. 740 – 748.

RESPONSIBILITY NOTICE

The authors are the only responsible for the printed material included in this paper.